Earth, Planets and Space

FULL PAPER Open Access

Penetration of the electric fields of the geomagnetic sudden commencement over the globe as observed with the HF Doppler sounders and magnetometers

Takashi Kikuchi[1*], Jaroslav Chum[2], Ichiro Tomizawa[3], Kumiko K. Hashimoto[4], Keisuke Hosokawa[5], Yusuke Ebihara[6], Kornyanat Hozumi[7] and Pornchai Supnithi[8]

Abstract

Using the HF Doppler sounders at middle and low latitudes (Prague, Czech Republic; Tucuman, Argentina; Zhongli, Republic of China, and Sugadaira, Japan), we observed the electric fields of the geomagnetic sudden commencement (SC) propagating near-instantaneously (within 10 s) over the globe. We found that the electric fields of the preliminary impulse (PI) and main impulse (MI) of the SC are in opposite direction to each other and that the PI and MI electric fields are directed from the dusk to dawn and dawn to dusk, respectively, manifesting the nature of the curl-free potential electric field. We further found that the onset and peak of the PI electric field are simultaneous on the day and nightsides (0545, 1250, 1345 MLT) within the resolution of 10 s. With the magnetometer data, we confirmed the near-instantaneous development of the ionospheric currents from high latitudes to the equator and estimated the location of the field-aligned currents that supply the ionospheric currents. The global simultaneity of the electric and magnetic fields does not require the contribution of the magnetohydrodynamic waves in the magnetosphere nor in the F-region ionosphere. The global simultaneity and day–night asymmetry of the electric fields are explained with the ionospheric electric potentials transmitted at the speed of light by the TM_0 mode waves in the Earth-ionosphere waveguide.

Keywords: HF Doppler sounder, Penetration electric field, Geomagnetic sudden commencement, Preliminary impulse, Global simultaneous onset, TM_0 mode wave in the earth-ionosphere waveguide, Polar-equatorial ionospheric currents

Introduction

PI and MI of SC

The geomagnetic sudden commencement (SC) is observed at low latitudes as a stepwise increase in the X/H-component of the magnetic field (DL: disturbance observed at low latitudes), which is caused by the magnetopause currents generated by the solar wind shock (Araki 1994). The DL is preceded by the preliminary impulse (PI) followed by the MI at high latitudes, caused by ionospheric Hall currents driven by the dusk-to-dawn and dawn-to-dusk electric fields, respectively. The PI is positive in the morning and negative in the afternoon, and vice versa for the MI (Araki 1994). The ionospheric Hall currents decrease the intensity with decreasing latitude because of the geometrical attenuation of the penetration electric field (Kikuchi Araki et al. 1978). This results in rare occurrence of the PI at low latitudes, but the PI appears again at the dayside equator (Matsushita 1962; Araki 1977), where the westward ionospheric

*Correspondence: kikuchi@isee.nagoya-u.ac.jp
[1] Institute for Space-Earth Environmental Research, Nagoya University, Furo-cho, Chikusa-ku, Nagoya, Japan
Full list of author information is available at the end of the article

currents are enhanced by the Cowling effect (Hirono 1952; Baker and Martin 1953). From the current circuit point of view, the equatorial Cowling currents are supplied by the field-aligned currents (FACs) via the Pedersen currents at middle and low latitudes (Kikuchi et al. 2001). The FACs of PI are supplied by the $\boldsymbol{F} \times \boldsymbol{B}$ currents on the magnetopause ($\boldsymbol{F}$: external force, $\boldsymbol{B}$: Earth's magnetic field) (Tamao 1964), which has been reproduced by the global magnetohydrodynamic (MHD) simulations (Slinker et al. 1999; Fujita et al. 2003a, b).

The PI occurs simultaneously at high latitudes and equator within the temporal resolution of 10 s, suggesting that the ionospheric electric field and currents are transmitted instantaneously from the polar ionosphere to the equator (Araki 1977). The wave mode enabling the instantaneous transmission is the zeroth-order transverse magnetic (TM_0) mode propagating at the speed of light in the Earth-ionosphere waveguide (Kikuchi Araki et al. 1978; Kikuchi and Araki 1979). Kikuchi (2014) replaced the waveguide with the finite-length lossy transmission line and showed that the onset of the PI is instantaneous, while the peak of the PI could be delayed by 10–20 s that is required to achieve quasi-steady currents in the highly conductive equatorial ionosphere. The instantaneous onset and delayed peak of the equatorial PI have been confirmed by Takahashi et al. (2015).

HF Doppler observations

The SC electric fields have been observed as the Doppler frequency of the HF radio signals reflected from the F-layer of the ionosphere at middle latitudes (Davies et al. 1962; Kanellakos and Villard 1962; Chan et al. 1962; Huang et al. 1973; Kikuchi et al. 1985, 2016; Kikuchi, 1986; Pilipenko et al. 2010; Hashimoto et al. 2020). The HF Doppler frequency increases at the arrival of the SC followed by a frequency decrease on the dayside [Davies et al. 1962; Kanellakos and Villard 1962; Chan et al. 1962; Huang et al. 1973], and vice versa on the nightside (Chan et al. 1962; Kanellakos and Villard 1962; Sastri and Subrahmanyam 1974; Kikuchi et al. 1985). The initial frequency increase on the dayside was explained in terms of the westward induction electric field proportional to dB/dt (Huang 1976) or by the Earthward motion of the ionospheric plasma caused by the compressional MHD waves (Pilipenko et al. 2010). Kikuchi et al. (1985) found, based on statistics of the SC-associated Doppler frequencies (SCF), that the SC electric fields are in opposite direction on the day and nightsides with the daytime polarity extending to the evening sector until 21 MLT. They suggested that the HF Doppler frequencies are caused by the dusk-to-dawn and dawn-to-dusk electric fields associated with the PI and MI, respectively, which were named the PFD (preliminary frequency deviation) and MFD (main frequency deviation), respectively. Kikuchi (1986) showed that the PFD started at nightside middle latitudes simultaneously with the PI at the afternoon high latitude within the temporal resolution of 10 s. Furthermore, Kikuchi et al. (2016) showed that the dayside ionosphere is not compressed downward by the arrival of the compressional waves, but moves upward during the period when the magnetosphere continued to be compressed. The upward motion of the dayside ionosphere was shown to be correlated with the increase in the equatorial electrojet (EEJ), which indicates that the eastward electric field propagates to the middle latitude via the polar ionosphere together with the ionospheric currents extending to the equator. Hashimoto et al. (2020) reported simultaneous observations of the MI electric field at Prague, Czech Republic and Oarai, Japan, located in the evening and post-midnight, respectively. The MI electric field was westward in the post-midnight, while eastward in the evening, showing the evening anomaly of the MI electric field found by Kikuchi et al. (1985). The evening anomaly of the SC electric fields agrees with the model calculations of the electric potentials supplied by the field-aligned currents in the polar ionosphere (Tsunomura 1999), in contrast to the properties of the compressional MHD waves in the magnetosphere.

Issues to be resolved

The PI and MI electric fields have been well studied as overviewed above, but the local time and latitude features of the PI have not been evaluated by simultaneous observations over the globe. In particular, near-instantaneous onset of the PI electric field at middle latitudes has not been confirmed with direct observation of the electric fields on the day and nightsides. In this paper, we show the simultaneity of the PI electric fields with the resolution of the data (10 s) on the day and nightsides with the SC event on 17 March, 2015. For this purpose, we used the HF Doppler sounders at Prague, Czech Republic and Tucuman, Argentina on the nightside, and at Sugadaira, Japan and Zhongli, Republic of China on the dayside. To confirm the instantaneous transmission of the ionospheric currents from high latitude to the equator, we used magnetometer data with the resolution of 1 s from College, Alaska; Husafell, Iceland; Memambetsu, Kakioka and Kanoya, Japan, and Phuket, Thailand, we further used the IMAGE magnetometer array data to identify the location of the FACs in the polar ionosphere that supply the ionospheric currents to the equator. With these data sets, we confirmed the near-instantaneous propagation of the PI electric fields over the globe, characterized by the opposite polarity on the day and night sides, manifesting the electric field being curl-free potential field rather than the inductive wave field. We discuss that the global

simultaneity matches the speed of light propagation of the TM_0 mode wave in the Earth-ionosphere waveguide.

HF Doppler sounders and magnetometers

We used the HF Doppler sounders at middle latitudes; Sugadaira, Japan (SGD, 27.89° geomagnetic latitude (GML)); Zhongli, Republic of China (ZHL, 14.37° GML); Prague, Czech Republic (PRG, 49.37° GML); and Tucuman, Argentina (TCM, − 17.07° GML) (Table 1). The HF Doppler sounder networks have been used to detect the atmospheric gravity and infrasound waves or ionospheric response to solar flares over Europe, Taiwan and South America (Chum et al. 2014; Chum and Podolská 2018; Chum et al. 2018a, b) and the stormtime electric fields penetrated over the western Pacific and Europe (Hashimoto et al. 2020). When the electric fields penetrate to the middle latitudes, we observe Doppler shifts in the HF radio frequency, Δf, which is caused by the drift motion of plasma with velocity, $\mathbf{v} = \mathbf{E} \times \mathbf{B}/\mathbf{B}^2$, where $\boldsymbol{E}$ and $\boldsymbol{B}$ are the electric field and ambient magnetic field, respectively. Thus, we have,

$$E = -\frac{cB}{2f \cos I \sin\theta}\Delta f, \tag{1}$$

where c, I and θ refer to the speed of light, inclination of $\boldsymbol{B}$ and elevation angle of the radio path to the reflection point at 300 km from the ground, respectively. Using the parameters listed in Table 1, we have the electric field at each station as,

1. SGD (f=5.006 MHz),

$$E = -2.17\Delta f[\mathrm{mV/m}] \tag{2}$$

2. Zhongli (f=6.57 MHz)

$$E = -1.12\Delta f[\mathrm{mV/m}] \tag{3}$$

3. Prague (f=3.59 MHz)

$$E = -4.39\Delta f[\mathrm{mV/m}] \tag{4}$$

4. Tucuman (f=4.63 MHz)

$$E = -0.75\Delta f[\mathrm{mV/m}] \tag{5}$$

The ionospheric currents flowing from high latitudes to the equator are observed with the magnetometers deployed at high latitudes and equator (Araki 1977; Kikuchi et al. 1996). We used magnetometer data from the auroral latitudes; Husafell, Iceland (HUS, 69.2° GML) and College, Alaska (CMO, 65.5° GML), from the middle latitudes, Memambetsu (MMB, 35.7° GML), Kakioka (KAK, 27.8° GML) and Kanoya (22.3° GML), Japan, and from the equator, Phuket, Thailand (PKT, −1.53° GML) (Table 2). The equatorial ionospheric currents are intensified by the Cowling effects (Hirono 1952), which enhance the PI and MI currents overwhelming the DL due to the magnetopause currents. To identify the location of the FACs that supply the ionospheric currents, we used the IMAGE (International Monitor for Auroral Geomagnetic Effects) magnetometer array data (Table 3). The PI would change its polarity across some particular latitude over which the FACs flow in/out, since the PI is caused by the Hall current vortices surrounding the FACs (Tamao 1964; Araki 1994).

SC event on 17 March 2015

HF Doppler observations of the PI and MI electric fields

The SC occurred at 0445 UT on 17 March, 2015, when the solar wind shock compressed the magnetosphere. Figure 1 shows the solar wind OMNI data provided by NASA at Coordinated Data Analysis Web (https://cdaweb.sci.gsfc.nasa.gov); the solar wind flow pressure, solar wind electric field as well as the geomagnetic indices; SYM-H, AU and AL provided by the WDC for Geomagnetism, Kyoto (http://wdc.kugi.kyoto-u.ac.jp/wdc/Sec3.html). The stepwise increase in the SYM-H is the SC caused by the sudden increase in the solar wind pressure. The AU and AL indices look like a mirror image, which indicates that the ionospheric currents at auroral

Table 1 List of the HF Doppler sounders in Japan, Argentina, Czech Republic and Republic of China

Station name	Country	Frequency (MHz)	Geographic coordinate (deg)		Geomagnetic coordinate (deg)		Distance (km)	Elevation angle (deg)
			Latitude	Longitude	Latitude	Longitude		
Sugadaira SGD	Japan	5.006	36.52	138.32	27.89	−152.06	146	75.7
Zhongli ZHL	Republic of China	6.57	23.95	120.93	14.37	−167.22	82	82.2
Prague PRG	Czech Republic	3.594	50.04	14.48	49.37	98.51	7	89.3
Tucuman TCM	Argentina	4.63	−26.84	−65.23	−17.07	6.90	74	83.0

Table 2 List of the INTERMAGNET, SEALION, and NIPR Magnetometers

Station	Country	Geographic (deg)		Geomagnetic (deg)		MLT UT +
		Latitude	Longitude	Latitude	Longitude	
Intermagnet https://www.intermagnet.org/data-donnee/download-eng.php						
College CMO	USA	64.87	−147.86	65.46	−96.22	12.7
Memambetsu MMB	Japan	43.91	144.19	35.72	−147.77	9.4
Kakioka KAK	Japan	36.23	140.19	27.76	−150.33	9.2
Kanoya KNY	Japan	31.42	130.88	22.30	−158.39	8.7
Sealion https://aer-nc-web.nict.go.jp/sealion/index.html						
Phuket PKT	Thailand	8.09	98.32	−1.53	171.02	6.4
NIPR http://polaris.nipr.ac.jp/~uap-mon/uapm/uapm_new_top.html						
Husafell HUS	Iceland	64.67	−21.03	69.20	71.68	−0.6

Table 3 IMAGE magnetometer chain stations

Code	Name	Geographic		Corrected Geomagnetic	
		Lat	Lon	Lat	Lon
NAL	Ny Ålesund	78.92	11.95	75.25	112.08
LYR	Longyearbyen	78.20	15.82	75.12	113.00
HOR	Hornsund	77.00	15.60	74.13	109.59
BJN	Bear Island	74.50	19.20	71.45	108.07
SOR	Sørøya	70.54	22.22	67.34	106.17
MAS	Masi	69.46	23.70	66.18	106.42
MUO	Muonio	68.02	23.53	64.72	105.22
PEL	Pello	66.90	24.08	63.55	104.92
OUJ	Oulujärvi	64.52	27.23	60.99	106.14
HAN	Hankasalmi	62.25	26.60	58.69	104.54
NUR	Nurmijärvi	60.50	24.65	56.89	102.18
TAR	Tartu	58.26	26.46	54.47	102.89

latitudes are the DP2-type currents driven by the dawn-to-dusk electric field of the main impulse (MI) of SC. The DP2 currents are composed of clockwise and counter-clockwise current vortices in the morning and afternoon sectors, respectively, and of the eastward currents at the dayside equator (Nishida 1968). The solar wind electric field was negative (~ −5 mV/m) prior to the SC and changed further negative (~ −3 mV/m) during the SC, which suggests that the SC electric fields are solely caused by the solar wind pressure with no enhanced Region-1 field-aligned currents.

Figure 2 shows the HF Doppler frequency deviations of the PI and MI (hereafter, we use the PFD and MFD, respectively) observed at PRG (3.59 MHz), TCM (4.63 MHz), SGD (5 MHz) and ZHL (6.57 MHz). The PFD started to decrease at 0445:20 s UT on the nightside; PRG (0545 MLT) and TCM (0025 MLT), while the PFD increased on the dayside; SGD (1345 MLT) and ZHL (1250 MLT) at the same time as on the nightside within the resolution of 10 s. The PFD reached the peak at 0445:40-50 s UT, followed by the positive/negative MFD with peaks at 0446:40-60 s UT on the nightside/dayside. The simultaneous observations on the day and nightsides help to confirm that the PFD and MFD are caused by the dusk-to-dawn and dawn-to-dusk electric potential fields supplied by the pair of FACs in the polar ionosphere. Furthermore, the simultaneous onset of the PFD suggests near-instantaneous propagation of the electric potentials from the polar ionosphere to the middle latitudes on both the day and nightsides.

Figure 3 shows the electric fields converted from the HF Doppler frequencies with Eqs. (2)–(5). The electric fields of the PI and MI at PRG are + 3.0 and -7.8 mV/m (+ refers to eastward), respectively, which are much larger than those at TCM (+ 0.2, -0.4 mV/m), SGD (-0.8, + 1.1 mV/m) and ZHL (-0.8, + 1.2 mV/m). The large amplitude at PRG is due to the latitude (49.4° GML) being higher than the other stations (< 27.9° GML) and is due to that PRG was in the pre-dawn sector. The electric field in the pre-dawn sector is much larger than those in the afternoon sector as shown by the model calculations of the ionospheric electric field (Senior and Blanc 1984; Tsunomura and Araki 1984; Tsunomura 1999). The small electric field at TCM may also be due to the local time dependence of the penetration electric fields with the evening anomaly extending to the midnight where

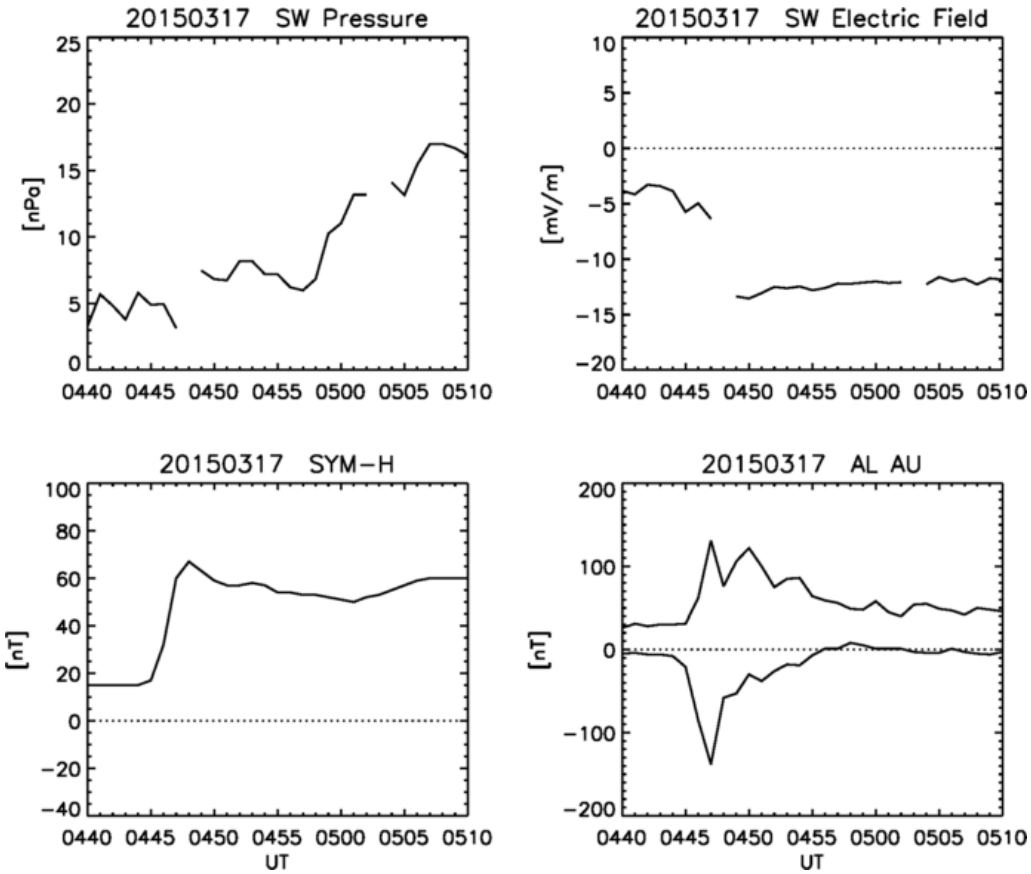

Fig. 1 Solar wind flow pressure (top left) and electric field (top right) at the magnetopause (from the OMNI provided by NASA), and geomagnetic SYM-H (bottom left), AL and AU (bottom right) indices as derived from the ground magnetometer data (from WDC for Geomagnetism, Kyoto) during the geomagnetic sudden commencement on 17 March, 2015

TCM was located. The model calculation by Nopper and Carovillano (1978) showed that the electric field crosses zero at around 00 MLT as in Fig. 1b of their paper. This model could be useful to explain the small amplitude at TCM.

SCs at auroral latitudes

The SC electric fields at middle latitudes have been explained as being associated with ionospheric currents flowing from high latitudes to the equator (Kikuchi et al. 2016). To confirm this mechanism, we used magnetometer data deployed from the auroral latitudes to the equator. Figure 4 shows the SC recorded at Husafell (HUS), Iceland (0410 MLT) and College (CMO), Alaska (1730 MLT), which are composed of the negative PI and positive MI in the X-component. Since the upward FAC of the PI is located in the morning sector (10 MLT) (Fujita et al. 2003a), the X and Y of the PI FACs calculated with the Biot-Savart's law are negative and positive in the pre-dawn sector as was recorded at HUS. In the afternoon sector, on the other hand, the DP2-type ionospheric currents develop during the PI (Araki 1994), which produce the negative PI in the X-component as was recorded at CMO. The PI started at 0445:20 s at the two auroral latitude stations, separated by 11 h in local time. Furthermore, the onset of the PI is simultaneous with the PFD at middle and low latitudes (Fig. 2), which agrees with the scenario of the instantaneous propagation of the electric potential and currents from high latitudes to the middle latitude during the PI.

SCs at middle-equatorial latitudes

Figure 5 shows the SC recorded in the H- (solid curve) and D- components (dotted curve) at middle latitudes, Memambetsu (MMB), Kakioka (KAK) and Kanoya (KNY), Japan in the early afternoon (14 MLT) and at the equator, Phuket (PKT), Thailand in the pre-noon (11 MLT). The SC in H is basically the DL caused by the magnetopause currents as clearly observed at KNY and KAK. On the other hand, the negative PI and positive MI are superposed on the DL at PKT as well as at MMB with smaller magnitude. The PI at PKT started at 0445:20 s

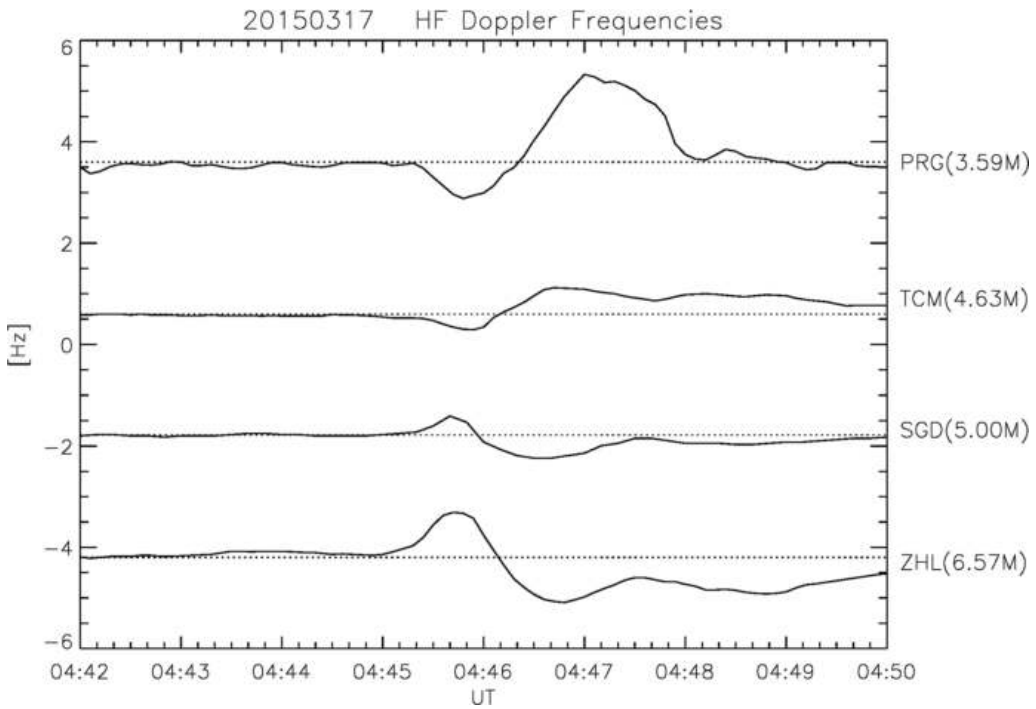

Fig. 2 HF Doppler frequencies observed during the SC at Prague (PRG, 3.59 MHz) and Tucuman (TCM, 4.63 MHz) on the nightside (0545, 0025 MLT) and at Sugadaira (SGD, 5.006 MHz) and Zhongli (ZHL, 6.57 MHz) on the dayside (1345, 1250 MLT). The HF Doppler frequencies are composed of the negative PFD and positive MFD on the nightside, and vice versa on the dayside

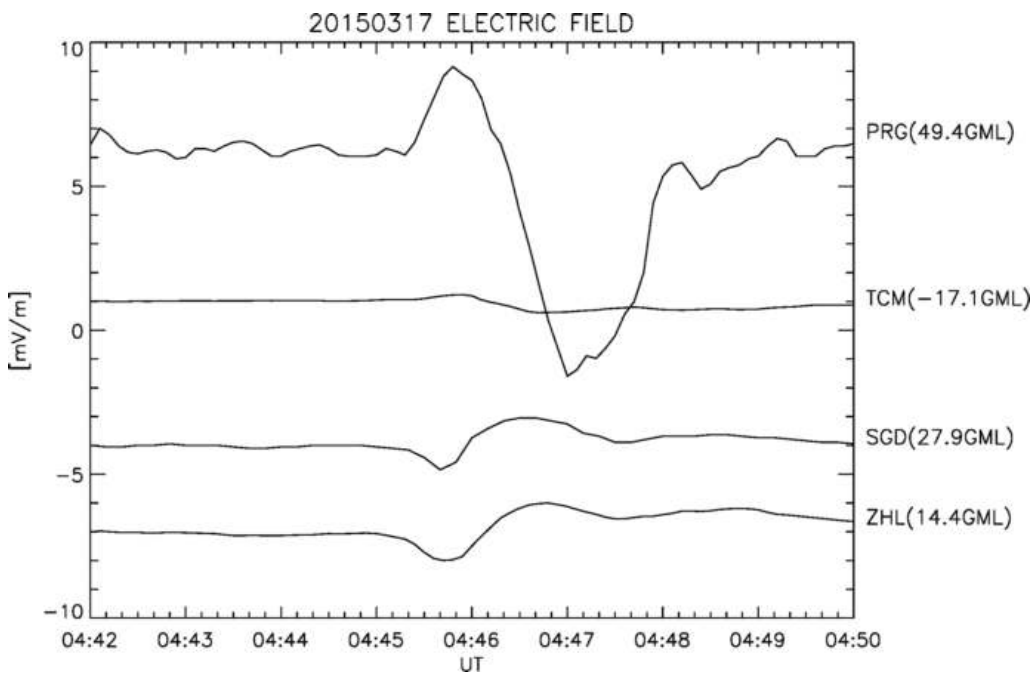

Fig. 3 Electric fields of the PI and MI of the SC converted from the HF Doppler frequencies observed at PRG (49.4° GML) and TCM (-17.1° GML) on the nightside, and at SGD (27.9° GML) and ZHL (14.4° GML) on the dayside. The local time features meet the dusk-to-dawn PI and dawn-to-dusk MI electric fields

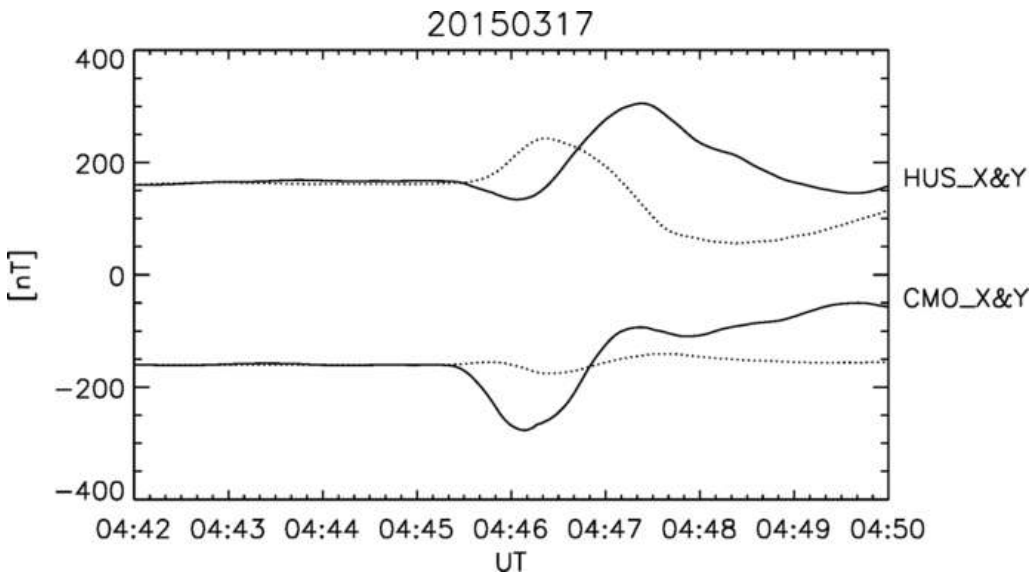

Fig. 4 SCs recorded in the X- and Y-components at Husafell, Iceland (HUS) and College, Alaska (CMO), located in the pre-dawn (0410 MLT) and afternoon (1730 MLT), respectively. The X and Y are plotted with the solid and dotted curves, respectively

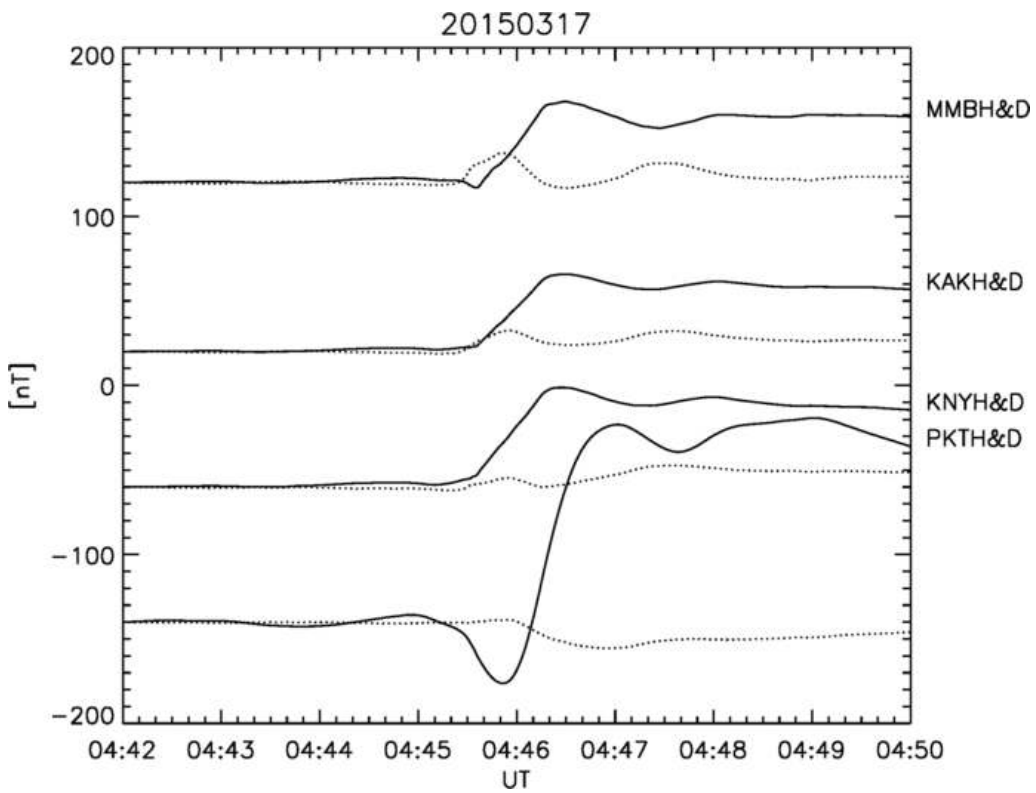

Fig. 5 SCs recorded at middle latitudes; Memambetsu (MMB, 35.72º GML), Kakioka (KAK, 27.76º GML) and Kanoya (KNY, 22.30º GML), Japan in the afternoon sector (14 MLT), and at the geomagnetic equator; Phuket, Thailand (PKT, -1.53º GML) in the pre-noon sector (11 MLT). The H- and D-components are plotted with the solid and dotted curves, respectively. The SC is composed of the DL at middle latitudes, while the PI and MI are superposed on the DL at the equator

UT and peaked at 0445:50 s UT, simultaneously with the onset and peak of the PFD at SGD and ZHL (Fig. 2). The PI in the D-component (dotted curve) is positive at MMB and KAK, starting at the same time as the PI at PKT. If the PI FAC flows into the polar ionosphere at 15 MLT and moves slowly toward the dusk terminator (Fujita et al. 2003a), the clockwise Hall currents surrounding the downward FAC as well as the Biot-Savart's magnetic field of the FAC would cause negative D at MMB located at 14 MLT. On the other hand, the downward FAC is connected with the westward equatorial Cowling currents by the southward Pedersen currents in the afternoon sector as depicted schematically in Fig. 7 of Kikuchi et al. (2001). The positive D-component shown in the present paper never meets the Hall currents, but meets the southward Pedersen currents that takes the part in the current circuit from the FACs to the equatorial Cowling currents. Consequently, the PI electric field and currents propagate near-instantaneously over the globe. It is interesting to note that the peak of the PI at CMO and HUS (0446:10sUT) is delayed from the peak at PKT (0445:50 s UT) by 20 s. As discussed by Kikuchi and Araki (2002), the peak time of the equatorial PI is not solely associated with the PI currents in the polar ionosphere, but a result of superposition of the DL, PI and MI. The PI tends to decrease as the DL and MI become overwhelming. Likewise, the PI at MMB with small magnitude and short duration is due to the overwhelming DL. According to the global simulation of the PI and MI FACs (Fujita et al. 2003a, b), the PI FACs develop on the dayside (10, 15 MLT) and move poleward and toward the terminator, followed by the MI FACs developing equatorward of the PI FACs. Both the PI and MI FACs are active for a while, even during the time periods when the MI is dominant at the equator. The PI FAC may have caused the longer duration of the PI at high latitude, depending on the location of the station relative to the PI FAC. Recent global MHD simulations further showed that the superposition of the magnetic fields produced by the ionospheric currents, magnetopause currents and field-aligned currents results in the duration of 1 min for the PI at middle latitudes, while the duration is longer (2 min) at high latitudes (Tanaka et al. 2020).

Hall current vortex signatures with IMAGE magnetometer data

The FACs of the PI and MI have been estimated from the equivalent currents of the ground magnetic field variations which change their polarity across the FACs (Kikuchi et al. 2016). Figure 6 shows the X- and Y-components of the magnetic field at the IMAGE magnetometer stations located in the 07 MLT meridian. The PI in Y-component (right panel) is positive at all stations, starting at 0445: 20 s, simultaneously with the PFD at middle

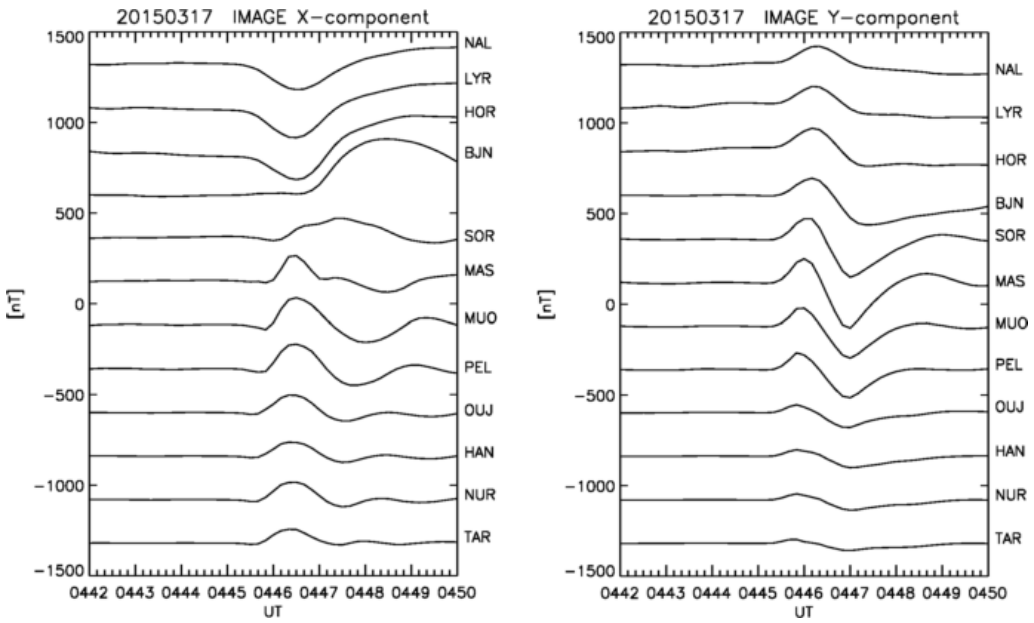

Fig. 6 SCs recorded in the X- and Y-components of the magnetic field at the IMAGE magnetometer array stations deployed in the morning sector (07 MLT) from the polar cap, Ny Alesund (NAL, 75.25° CGML) to middle latitude, Tartu (TAR, 54.47° CGML). The PI in X is positive at lower latitudes, while negative at higher latitudes from Bear Island (BJN, 71.45° CGML). In contrast, the PI in Y is positive at all stations. The latitudinal features of the X and Y meet the dawnside part of the counter-clockwise Hall current vortex surrounding the upward FAC

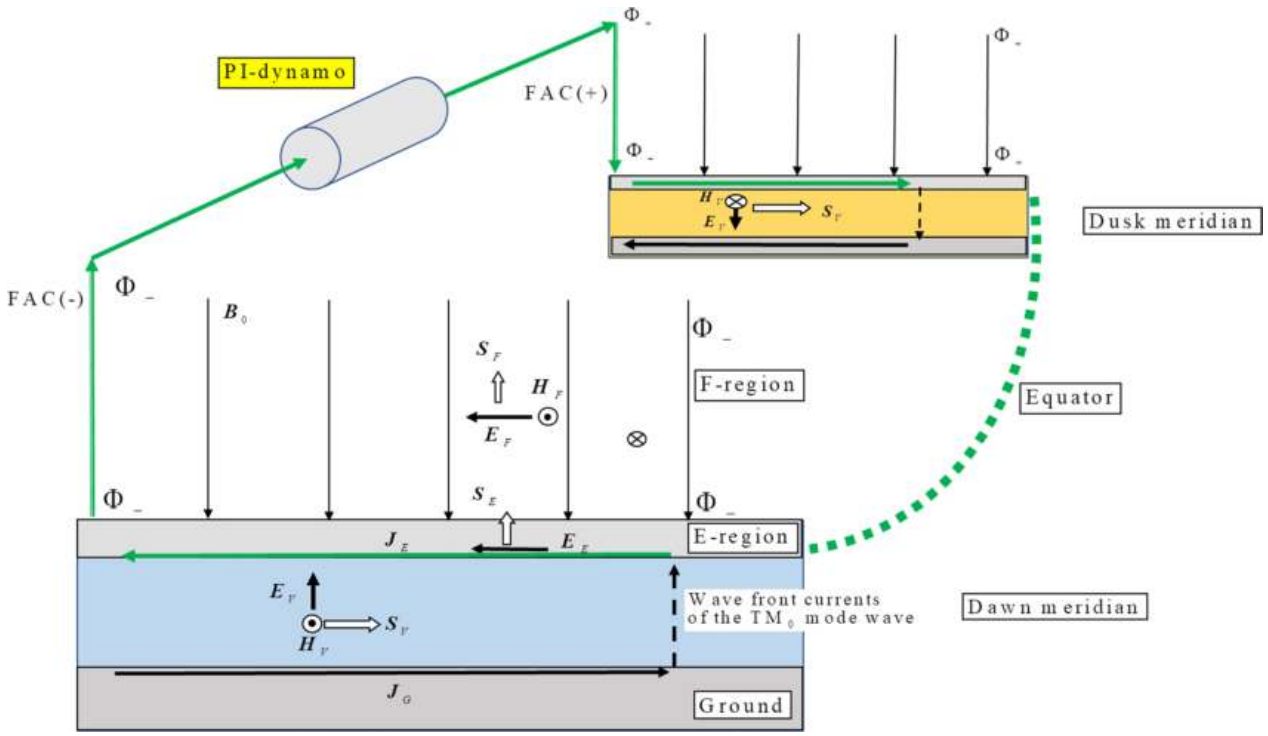

Fig. 7 Schematic diagram of a pair of the Earth-ionosphere waveguide for the positive electric potential (Φ_+) on the duskside and negative potential (Φ_-) on the dawnside, supplied by the PI dynamo through the field-aligned currents in the magnetosphere. The electric potentials are transmitted from the polar ionosphere

latitudes. The global MHD simulation showed that the upward FAC develops at 10 MLT and moves poleward and toward the terminator (Fujita et al. 2003a). The positive Y-component may be caused by the southward currents in the dawnside part of the counter-clockwise Hall current vortex surrounding the upward FAC. The PIs in X-component (left panel), on the other hand, are negative at higher latitudes (HOR-NAL), while positive at lower latitudes (MAS-NUR). The negative/positive X may be caused by westward/eastward currents at higher/lower latitude part of the Hall current vortex. It is to be noted that the Pedersen currents could never cause the reversal in the X-component along the meridian, even if there were zonal electric fields crossing the magnetometer array. The peaks of the PI in both the X- and Y-components are delayed by up to 30 s as the latitude increases, which may be associated with the poleward motion of the simulated FAC. From the latitudinal features of the PI, we infer that the upward FAC was located at the latitude of BJN and eastward of the IMAGE magnetometer array.

Discussion

Excitation of waves in the magnetosphere

When the magnetosphere is compressed by the increase in the solar wind flow pressure, the eastward magnetopause currents are intensified, producing increases in the magnetic field inside the magnetosphere. Tamao (1964) formulated the generation and propagation of the SC with the following equation:

$$\nabla^2 A - \frac{1}{V_A^2}\frac{\partial^2 A}{\partial t^2} = -\frac{\mu_0}{B^2} F \times B, \tag{6}$$

where $\boldsymbol{F}$, μ_0, $\boldsymbol{A}$, and V_A denote the external force, magnetic permeability, magnetic vector potential, and Alfven speed, respectively. The external force drives the eastward currents, $F \times B/B^2$, on the magnetopause, which creates $\boldsymbol{A}$ inside the magnetosphere.

Two propagation modes

With the Eq. (6), Tamao (1964) discussed propagation of isotropic (compressional) mode and transverse (Alfven) mode waves, as described by the following Eqs. (7) and (8), respectively.

$$\left(\nabla^2 - \frac{1}{V_A^2}\frac{\partial^2}{\partial t^2}\right)\nabla_z \times A_\perp = -\frac{\mu_0}{B^2}\nabla_z \times (F \times B) \tag{7}$$

$$\left(\frac{\partial^2}{\partial z^2}-\frac{1}{V_A^2}\frac{\partial^2}{\partial t^2}\right)\nabla\cdot A_\perp=-\frac{\mu_0}{B^2}\nabla\cdot(F\times B) \tag{8}$$

Compressional waves transporting the DL

Equation (7) describes that the compressional wave transports the increase in the magnetic field parallel to the ambient magnetic field, $b_z=\nabla_z\times A_\perp$, toward the Earth, which is observed as the DL at the middle and low latitudes (Fig. 5). The compressional waves propagate even to the nightside (Wilken et al. 1982) and provide the westward electric field responsible for the compression of the magnetosphere at all local times (Shinbori et al. 2004).

Alfven waves transporting electric potentials and FACs

Equation (8) describes the propagation of the Alfven waves transporting the electric potentials and FACs of the PI down the magnetic field lines to the polar ionosphere. To derive the equations for the electric potentials, we use the following Lorentz condition (9) and continuity equation between the charge density and current density (10).

$$\nabla\cdot A_\perp+\frac{1}{V_A^2}\frac{\partial\Phi}{\partial t}=0 \tag{9}$$

$$\nabla\left(\frac{F\times B}{B^2}\right)=-\frac{\partial\sigma}{\partial t}, \tag{10}$$

where Φ and σ denote the electric potential and charges created by the magnetopause currents. From Eqs. (8)–(10), we obtain the following Eq. (11) for Φ.

$$\left(\frac{\partial^2}{\partial z^2}-\frac{1}{V_A^2}\frac{\partial^2}{\partial t^2}\right)\Phi_\pm=\mp\frac{1}{\varepsilon}\sigma, \tag{11}$$

The positive and negative potentials propagate to the auroral ionosphere with field-aligned currents flowing into the afternoon (14 h) and out from the morning (10 h), respectively (Fujita et al. 2003a). After arriving at the polar ionosphere, the electric potentials drive the ionospheric Hall currents with counter-clockwise and clockwise directions in the morning and afternoon sectors, respectively, which cause the negative PI at CMO in the afternoon and positive PI at the IMAGE stations in the morning. The negative H and positive D at HUS, on the other hand, may be magnetic fields produced by the upward FAC as calculated with the Biot-Savart's law. The magnetic fields of the PI FACs have been observed even at middle latitudes on the dayside (Kikuchi et al. 2001).

Propagation of ionospheric potentials to low latitudes

We now have positive and negative potentials at the feet of the downward and upward FACs in the afternoon and morning sectors, respectively. The electric potentials are transmitted by the TM_0 mode waves propagating at the speed of light in the Earth-ionosphere waveguide (Kikuchi 2014). Figure 7 shows a schematic diagram of two sets of the Earth-ionosphere waveguide for the negative (blue) and positive (orange) potentials supplied by the PI dynamo to the dawnside and duskside, respectively. The electric potentials provide vertical electric fields below the ionosphere at the feet of the FACs, which are transmitted at the speed of light by the TM_0 mode waves. The propagating TM_0 modes carry electric currents in the ionosphere and on the surface of the ground, which are connected by the displacement currents on the propagating wave front (Kikuchi Araki et al. 1978). The positive and negative potentials meet and cancel each other at the noon–midnight meridian, which enables us to replace the waveguide with the finite-length lossy transmission line (Kikuchi 2014). Kikuchi (2014) showed that the steady-state ionospheric currents are achieved with time constants of a few to 20 s, depending on the ionospheric conductivity. The time constant is short enough for us to consider the ionospheric currents being steady during the PI and MI. We can calculate the distribution of the electric potentials by solving the current continuity equation with the FACs as an input as was done in the previous papers (Nopper and Carovillano 1978; Tsunomura and Araki 1984; Senior and Blanc 1984; Tsunomura 1999).

The ionospheric potentials disseminated in the global ionosphere further propagate upward to the F-region by the Alfven waves. Under the daytime condition where the ionospheric conductance (e.g., 30 mho, Tsunomura 1999) is much larger than the Alfven conductance, $1/\mu_0 V_A$ (<1 mho for V_A=1000 km/s), the electric potentials propagate upward with no attenuation (Kikuchi and Araki 1979). The PI electric field further propagates to the inner magnetosphere as observed by the spacecrafts (Nishimura et al. 2010).

It should be stressed that the positive and negative electric potentials spread over the global E-region together with the electric currents supplied by the FACs. Thus, the electric fields are curl-free potential field as being divergent from/convergent to the downward/upward FAC. The curl-free electric fields have been validated as the electric potential field with the opposite directions on the day and nightsides, as shown in Fig. 3.

The vertical electric field in the waveguide takes part in transmitting the energy from the polar region to middle latitudes and the horizontal electric field in the E-region takes part in transmitting the energy to the F-region and

above, while a fraction of the energy is consumed in the E-region. This mechanism well explains the good correlation between the PFD at middle latitudes (Fig. 2) and PI at the equator (Fig. 5). Details of the transmission mechanism of the electric potentials are described in Kikuchi (2014).

Local time dependence of the electric potentials

It has been shown that the positive PFD and negative MFD were observed in the day and evening (-21 MLT) (Kikuchi et al. 1985), manifesting the evening anomaly of the penetration electric fields. The evening anomaly is characterized by the enhancement in the magnitude compared to those on the dayside (Kikuchi et al. 2016). The evening anomaly of the penetration electric fields have been shown for the DP2 fluctuation events (periods = 20–40 m) observed with the HF Doppler sounders at the equator (Abdu et al. 1998). Tsunomura (1999) pointed out that the global potential pattern is distorted by the Hall effects and day–night inhomogeneity of the ionospheric conductivities. The evening anomaly spans until pre-midnight; 21–22 MLT in the observations (Kikuchi et al. 1985) and 21–24 MLT in the model calculations (Nopper and Carovillano 1978; Tsunomura and Araki 1984; Senior and Blanc 1984). Thus, it would be reasonable to expect that the SC electric fields cross zero in the midnight, resulting in small magnitude of the electric fields as observed at TCM (Fig. 3).

Conclusion

With the HF Doppler sounders at middle and low latitudes (Prague, Czech Republic; Tucuman, Argentina; Zhongli, Republic of China; and Sugadaira, Japan), we observed the electric fields of the SC simultaneously on the day and nightsides (0025, 0545, 1250, 1345 MLT). We summarize our findings on the property of the SC electric fields derived from the HF Doppler observations as listed in the following items, 1, 2 and 3. The findings are supported by magnetometer observations deployed from high latitude to the equator as in the items, 4 and 5. The property of the electric field is clarified with the aid of the waveguide model in the item, 6.

1. We found that the electric fields of the preliminary impulse (PI) and main impulse (MI) of the SC are in opposite direction to each other on both the day and nightsides.
2. The PI and MI electric fields on the dayside are in opposite direction to those on the nightside, which is a property of the curl-free potential electric field diverging from/converging to the field-aligned currents.
3. We found that the onset and peak of the PI electric field are simultaneous on the day and nightsides within the resolution of 10 s.
4. With the high latitude-to-equatorial magnetometer chain data, we confirmed that the midlatitude electric fields are associated with ionospheric currents developed near-instantaneously from high latitudes to the equator.
5. The latitudinal dependence of the PI along the IMAGE magnetometer array helped to estimate the latitude of the upward field-aligned currents in the morning sector.
6. The simultaneous onset and curl-free property of the PI electric field does not require the contribution of the compressional MHD waves in the magnetosphere nor in the F-region ionosphere. The electric fields should be associated with the ionospheric potentials transmitted at the speed of light by the TM_0 mode waves in the Earth-ionosphere waveguide.

Abbreviations

HF: High frequency; SCF: SC-associated Doppler frequency; PFD: Preliminary frequency deviation; MFD: Main frequency deviation; SC: Geomagnetic sudden commencement; PI: Preliminary impulse; MI: Main Impulse; DL: Stepwise low latitude magnetic disturbance; EEJ: Equatorial electrojet; TM_0: Zeroth-order transverse magnetic; MHD: Magnetohydrodynamic; GML: Geomagnetic latitude; CGML: Corrected geomagnetic latitude.

Acknowledgements

The results presented in this paper rely on the HF Doppler sounder data collected at Prague, Tucuman, Zhongli and Sugadaira. Data from Tucuman and Zhongli were obtained in the collaboration with Universidad Nacional de Tucuman, Argentina and National Central University, Republic of China. The results rely on magnetometer data collected at College, Husafell, Memambetsu, Kakioka, Kanoya, Phuket, and IMAGE magnetometer array. We thank the US Geological Survey for data from College; National Institute of Polar Research, Tokyo for Husafell; Kakioka Magnetic Observatory, Japan Meteorological Agency for Memambetsu, Kakioka and Kanoya; and King Mongkut's Institute of Technology Ladkrabang (KMITL), Thailand for Phuket data. We thank the institutes who maintain the IMAGE Magnetometer Array: Tromsø Geophysical Observatory of UiT the Arctic University of Norway (Norway), Finnish Meteorological Institute (Finland), Institute of Geophysics Polish Academy of Sciences (Poland), GFZ German Research Centre for Geosciences (Germany), Geological Survey of Sweden (Sweden), Swedish Institute of Space Physics (Sweden), Sodankylä Geophysical Observatory of the University of Oulu (Finland), and Polar Geophysical Institute (Russia). We thank INTERMAGNET for promoting high standards of magnetic observatory practice (http://www.intermagnet.org). The AU, AL and SYM-H indices used in this paper were provided by the WDC for Geomagnetism, Kyoto (http://wdc.kugi.kyoto-u.ac.jp/wdc/Sec3.html). The OMNI solar wind data were obtained through the Coordinated Data Analysis Web (CDAWeb; http://cdaweb.gsfc.nasa.gov/).

Authors' contributions

TK contributed to the design and implementation of the study, to the analysis of the results and to the writing of the manuscript. JC contributed to selection of the SC event and performed observations with HF Doppler sounders in Prague, Tucuman and Zhongli. IT and KH performed observations with HF Doppler sounders in Sugadaira. KKH contributed to the analysis of the magnetometer data in binary format. KH and PS performed observations with the magnetometer at Phuket. YE contributed to the analysis of the electric

field with the global simulation model. All authors read and approved the final manuscript.

Funding
The works of TK and KKH are supported by the JSPS KAKENHI grant number JP22540461 and JP26400481 and the joint research program of the National Institute of Polar Research, Tokyo. The work of JC was supported under the grant 18-01969S by the Czech Science Foundation. The works of IT, KH, KKH and TK are supported by Hoso Bunka Foundation. The study of TK is supported by the grants-in-aid for Scientific Research (15H05815) of Japan Society for the Promotion of Science (JSPS) and the joint research programs of the Institute for Space-Earth Environmental Research, Nagoya University, and the KDK of the Research Institute for Sustainable Humanosphere, Kyoto University. The work of KH and the HF Doppler project in Japan are supported by the Takahashi Industrial and Economic Research Foundation and the Murata Science Foundation.

Availability of data and materials
1. HF Doppler: HF Doppler Sounding Experiment in Japan – HFDOPE, The University of Electro-Communications (http://gwave.cei.uec.ac.jp/~hfd/). 2. HF Doppler. The Institute of Atmospheric Physics of the Czech Academy of Science, (http://datacenter.ufa.cas.cz/). 3. Geomagnetic indices: World Data Center for Geomagnetism, Kyoto (http://wdc.kugi.kyoto-u.ac.jp/wdc/Sec3.html).4. Magnetometer data: Kakioka Magnetic Observatory (http://www.kakioka-jma.go.jp/obsdata/metadata/en). 5. Magnetometer data: SEALION, National Institute of Information and Communications, (https://aer-nc-web.nict.go.jp/sealion/index.html). 6. Magnetometer data: Data Center for Aurora, National Institute of Polar Research, (http://polaris.nipr.ac.jp/~uap-mon/uapm/uapm_new_top.html). 7. Magnetometer data: IMAGE (International Monitor for Auroral Geomagnetic Effects) (https://www.intermagnet.org/data-donnee/download-eng.php). 8. Magnetometer data: INTERMAGNET website (http://www.intermagnet.org). 9. Solar wind data of the OMNI Coordinated Data Analysis Web, NASA (https://cdaweb.sci.gsfc.nasa.gov).

Ethics approval and consent to participate
Not applicable.

Consent for publication
Not applicable.

Competing interests
No competing interests.

Author details
[1] Institute for Space-Earth Environmental Research, Nagoya University, Furo-cho, Chikusa-ku, Nagoya, Japan. [2] Department of the Ionosphere and Aeronomy, Institute of Atmospheric Physics, Czech Academy of Sciences, Prague, Czech Republic. [3] Center for Space Science and Radio Engineering, The University of Electro-Communications, 1-5-1 Chofugaoka, Chofu, Tokyo 182-8585, Japan. [4] School of Agriculture, Kibi International University, 370-1, Shichi-Sareo, Minamiawaji, Hyogo, Japan. [5] Department of Communication Engineering and Informatics, The University of Electro-Communications, 1-5-1 Chofugaoka, Chofu, Tokyo 182-8585, Japan. [6] Research Institute for Sustainable Humanosphere, Kyoto University, Gokasho, Uji, Koyto, Japan. [7] National Institute of Information and Communications Technology, 4-2-1 Nukui-kita, Koganei, Tokyo 184-8795, Japan. [8] Faculty of Engineering, King Mongkuts Institute of Technology Ladkrabang, Bangkok 10520, Thailand.

Received: 28 July 2020 Accepted: 26 December 2020
Published online: 06 January 2021

References

Abdu MA, Sastri JH, Lühr H, Tachihara H, Kitamura T, Trivedi NB, Sobral JHA (1998) DP 2 electric field fluctuations in the dusk-time dip equatorial ionosphere. Geophys Res Let 25(9):1511–1514
Araki T (1977) Global structure of geomagnetic sudden commencements. Planet Space Sci 25:373–384
Araki T (1994) A physical model of the geomagnetic sudden commencement, solar wind sources of magnetospheric ultra-low-frequency waves. Geophysical Monograph 81:183–200
Baker, W. G., and D. F. Martyn (1953), Electric currents in the ionosphere I. The conductivity, *Phil. Trans. R. Soc. London,* Ser.A 246, 281–294.
Chan KL, Kanellakos DP, Viilard OG Jr (1962) Correlation of short-period fluctuations of the earth's magnetic field and instantaneous frequency measurements. J Geophys Res 67:2066–2072
Chum J et al (2014) Propagation of gravity waves and spread F in the low-latitude ionosphere over Tucumán, Argentina, by continuous Doppler sounding: First results. J Geophys Res Space Physics 119:6954–6965. https://doi.org/10.1002/2014JA020184
Chum J, Urbář J, Laštovička J, Cabrera MA, Liu JY, Bonomi F, Fagre M, Fišer J, Mošna Z (2018a) Continuous Doppler sounding of the ionosphere during solar flares. Earth Planets Space 70:198. https://doi.org/10.1186/s40623-018-0976-4
Chum J, Liu J-Y, Podolská K, Šindelářová T (2018) Infrasound in the ionosphere from earthquakes and typhoons. J Atmos Sol Terr Phys 171:72–82. https://doi.org/10.1016/j.jastp.2017.07.022
Chum J, Podolská K (2018) 3D analysis of GW propagation in the ionosphere. Geophys Res Lett 45:11562–11571. https://doi.org/10.1029/2018GL079695
Davies K, Watts JM, Zacharisen DH (1962) A study of F2-layer effects as observed with a Doppler technique. J Geophys Res 67:601–609
Fujita, S., T. Tanaka, T. Kikuchi, K. Fujimoto, K. Hosokawa, and M. Itonaga (2003a), A numerical simulation of the geomagnetic sudden commencement: 1. Generation of the field-aligned current associated with the preliminary impulse, J. Geophys. Res., 108(A12), 1416, doi:https://doi.org/10.1029/2002JA009407.
Fujita, S., T. Tanaka, T. Kikuchi, K. Fujimoto, M. Itonaga (2003b), A Numerical Simulation of the Geomagnetic Sudden Commencement: 2. Plasma Processes in the Main Impulse, *J. Geophys. Res., 108*(A12), 1417, doi:https://doi.org/10.1029/2002JA009763.
Hashimoto KK, Kikuchi T, Tomizawa I, Hosokawa K, Chum J, Buresova D, Nose M, Koga K (2020) Penetration electric fields observed at middle and low latitudes during the 22 June 2015 geomagnetic storm. Earth Planets Space. https://doi.org/10.1186/s40623-020-01196-0
Hirono M (1952) A theory of diurnal magnetic variations in equatorial regions and conductivity of the ionosphere E region. J Geomag Geoelectr Kyoto 4:7–21
Huang Y-N, Najita K, Yuen P (1973) The ionospheric effects of geomagnetic sudden commencements as measured with an HF Doppler sounder at Hawaii. J Atmos Terr Phys 35:173–181
Huang Y-N (1976) Modeling HF Doppler effects of geomagnetic sudden commencements. J Geophys Res 81:175–182
Kanellakos DP, Villard OG Jr (1962) Ionospheric disturbances associated with the solar flare of September 28, 1961. J Geophys Res 67:2265–2277
Kikuchi T, Araki T, Maeda H, Maekawa K (1978) Transmission of polar electric fields to the Equator. Nature 273:650–651
Kikuchi T, Araki T (1979) Horizontal transmission of the polar electric field to the equator. J Atmosph Terrest Phys 41:927–936
Kikuchi T, Ishimine T, Sugiuchi H (1985) Local time distribution of HF Doppler frequency deviations associated with storm sudden commencements. J Geophys Res 90:4389–4393
Kikuchi T (1986) Evidence of transmission of polar electric fields to the low latitude at times of geomagnetic sudden commencements. J Geophys Res 91:3101–3105
Kikuchi T, Lühr H, Kitamura T, Saka O, Schlegel K (1996) Direct penetration of the polar electric field to the equator during a DP2 event as detected by the auroral and equatorial magnetometer chains and the EISCAT radar. J Geophys Res 101:17161–17173
Kikuchi T, Tsunomura S, Hashimoto K, Nozaki K (2001) Field-aligned current effects on midlatitude geomagnetic sudden commencements. J Geophys Res 106:15555–15565
Kikuchi T., and T. Araki (2002), Comment on "Propagation of the preliminary reverse impulse of sudden commencements to low latitudes" by P. J. Chi et al., *J. Geophys. Res., 107* (A12), 1473, doi:https://doi.org/10.1029/2001JA009220.
Kikuchi T (2014) Transmission line model for the near-instantaneous transmission of the ionospheric electric field and currents to the equator. J Geophys Res Space Physics. https://doi.org/10.1002/2013JA019515

Kikuchi T, Hashimoto KK, Tomizawa I, Ebihara Y, Nishimura Y, Araki T, Shinbori A, Veenadhari B, Tanaka T, Nagatsuma T (2016) Response of the incompressible ionosphere to the compression of the magnetosphere during the geomagnetic sudden commencements. J Geophys Res Space Physics. https://doi.org/10.1002/2015JA022166

Matsushita S (1962) On geomagnetic sudden commencements, sudden impulses, and storm durations. J Geophys Res 67:3753–3777

Nishida A (1968) Coherence of geomagnetic DP2 magnetic fluctuations with interplanetary magnetic variations. J Geophys Res 73:5549–5559

Nishimura Y, Kikuchi T, Shinbori A, Wygant J, Tsuji Y, Hori T, Ono T, Fujita S, Tanaka T (2010) Direct measurements of the Poynting flux associated with convection electric fields in the magnetosphere. J Geophys Res 115:A12212. https://doi.org/10.1029/2010JA015491

Nopper RW, Carovillano RL (1978) Polar equatorial coupling during magnetically active periods. Geophys Res Lett 5(8):699–702

Pilipenko V, Fedorov E, Yumoto K, Ikeda A, Sun TR (2010) An analytical model for Doppler frequency variations of ionospheric HF sounding caused by SSC. J Geophys Res 115:A10228. https://doi.org/10.1029/2010JA015403

Sastri JH, Subrahmanyam CV (1974) Sudden frequency deviations due to immediate effect of geomagnetic sudden commencements. J Geornagn Geoelectr 26:385

Senior C, Blanc M (1984) On the control of magnetospheric convection by the spatial distribution of ionospheric conductivities. J Geophys Res 89:261–284

Shinbori A, Ono T, Iizima M, Kumamoto A (2004) SC related electric and magnetic field phenomena observed by the Akebono satellite inside the plasmasphere. Earth Planets Space 56:269–282

Slinker SP, Fedder JA, Hughes WJ, Lyon JG (1999) Response of the ionosphere to a density pulse in the solar wind: simulation of traveling convection vortices. Geophys Res Lett 26:3549–3552

Takahashi N, Kasaba Y, Shinbori A, Nishimura Y, Kikuchi T, Ebihara Y, Nagatsuma T (2015) Response of ionospheric electric fields at mid-low latitudes during sudden commencements. J Geophys Res Space Physics 120:4849–4862. https://doi.org/10.1002/2015JA021309

Tamao T (1964) The structure of three-dimensional hydromagnetic waves in a uniform cold plasma. J Geomag Geoelectr 48:89–114

Tanaka, T., Ebihara, Y., Watanabe, M., Den, M., Fujita, S., Kikuchi, T., K. K. Hashimoto, and R. Kataoka (2020). Reproduction of ground magnetic variations during the SC and the substorm from the global simulation and Biot-Savart's law. *Journal of Geophysical Research: Space Physics*, *125*, e2019JA027172. https:// doi.org/https://doi.org/10.1029/2019JA027172

Tsunomura S, Araki T (1984) Numerical analysis of equatorial enhancement of geomagnetic sudden commencement. Planet Space Sci 32:599–604

Tsunomura S (1999) Numerical analysis of global ionospheric current system including the effect of equatorial enhancement. Ann Geophys 17:692–706. https://doi.org/10.1007/s00585-999-0692-2

Wilken B, Goertz CK, Baker DN, Higbie PR, Fritz TA (1982) The SSC on July 29, 1977 and its propagation within the magnetosphere. J Geophys Res 87:5901–5910

Publisher's Note